PAPER

Check for updates

A chemosensor for micro- to nano-molar detection of Ag$^+$ and Hg^{2+} ions in pure aqueous media and its applications in cell imaging†

Jitendra P. Nandre,[a] Samadhan R. Patil,[a] Suban K. Sahoo, [iD][b]
Chullikkattil P. Pradeep, [iD][c] Andrei Churakov,[d] Fabiao Yu,[e] Lingxin Chen, [iD] *[e]
Carl Redshaw, [iD][f] Ashok A. Patil*[a] and Umesh D. Patil [iD] *[g]

The pyridine substituted thiourea derivative **PTB-1** was synthesized and characterized by spectroscopic techniques as well as by single crystal X-ray crystallography. The metal ion sensing ability of **PTB-1** was explored by various experimental (naked-eye, UV-Vis, fluorescence, mass spectrometry and ^{1}H NMR spectroscopy) and theoretical (B3LYP/6-31G**/LANL2DZ) methods. **PTB-1** exhibited a highly selective naked-eye detectable color change from colorless to dark brown and UV-Vis spectral changes for the detection of Ag$^+$ with a detection limit of 3.67 μM in aqueous medium. The detection of Ag$^+$ ions was achieved by test paper strip and supported silica methods. In contrast, **PTB-1** exhibited a 23-fold enhanced emission at 420 nm in the presence of Hg^{2+} ions with a nano-molar detection limit of 0.69 nM. Finally, the sensor **PTB-1** was applied successfully for the intracellular detection of Hg^{2+} ions in a HepG2 liver cell line, which was monitored by the use of confocal imaging techniques.

Introduction

The synthesis and development of colorimetric and fluorescence chemosensors for heavy transition metal ions is gaining significant impetus due to their biological and environmental importance.[1–5] Among the transition metal ions, Ag$^+$ and Hg^{2+} ions have attracted considerable attention. The excessive intake and long-term accumulation of silver ions can lead to insoluble precipitates in the eyes and skin[6] and also can deactivate the normal functions of sulfhydryl enzymes.[7–9] Regular feasting of Ag$^+$ can cause anemia, growth

retardation, cardiac enlargement and degenerative changes in animals.[10] In addition, very strong Ag$^+$ ion recognition is essential for ^{111}Ag-based radio immunotherapy[11,12] and is useful for the recovery of Ag$^+$ from waste water, the latter mostly results from the photographic industries. However, the Ag$^+$ ion has only moderate coordination ability which makes it quite difficult to be separated from other chemically similar metal ions.

Additionally, mercury has been considered as the most toxic metal ion amongst the heavy transition metal ions to humans,[13–15] and causes severe neurotoxic, immunotoxic and genotoxic effects. Mercury contamination of ecosystems occurs through a number of sources, which include volcanic and oceanic discharges, burning of fossil fuels and solid waste incineration.[16,17] Mercury can be accumulated in the human body through the food chain. When it is accumulated in the human body, it can cause serious and lasting damage to the kidneys, endocrine system, brain, nervous system and immune system when present at a very low concentration.[18,19]

At present, a number of methods have been developed to detect Ag$^+$ and Hg^{2+} ions such as inductively coupled plasma detectors, inductively coupled plasma mass spectrometry (ICP-MS), fluorescence anisotropy assays, quantum dot based assays, atomic absorption spectrometry (AAS) and inductively coupled plasma atomic emission spectrometry (ICP-AES).[20–22] Although these technologies can detect Ag$^+$ and Hg^{2+} ions selectively with high sensitivity, they require exclusive and sophisticated instrumentation, highly trained hands and

[a]*Department of Chemistry, Z. B. Patil College, Deopur, Dhule – 424 002, MS, India*
[b]*Department of Applied Chemistry, S. V. National Institute Technology, Surat-395007, Gujrat, India*
[c]*School of Basic Sciences, Indian Institute of Technology Mandi, Mandi, Himachal Pradesh, 175001, India*
[d]*Institute of General and Inorganic Chemistry, Russian Academy of Sciences, Leninskii prosp. 31, Moscow 119991, Russian Federation*
[e]*Key Laboratory of Coastal Zone Environmental Processes and Ecological Remediation, Yantai Institute of Coastal Zone Research, Chinese Academy of Sciences, Yantai, Shandong, 264003, China*
[f]*Department of Chemistry, School of Mathematics and Physical Sciences, University of Hull, Cottingham Road, Hull, HU6 7RX, UK*
[g]*Department of Chemistry, S.S.V.P.S's L. K. Dr P. R. Ghogrey Science College, Dhule-424 001, MS, India*

†Electronic supplementary information (ESI) available: Details about spectra and characterization data including IR, NMR, mass, crystallographic data and DFT data. CCDC 986043. For ESI and crystallographic data in CIF or other electronic format see DOI: 10.1039/c7dt02524f

complex sample-preparation steps, which are major blockages in their everyday use. In contrast, the naked-eye detection method allows detection up to micro/submicromolar levels and that too without involving any expensive/sophisticated instruments. Silver and mercury are normally found as ions (Ag^+ and Hg^{2+}) in water. Therefore, there is a high demand for highly selective and sensitive chemosensors for detecting Ag^+ and Hg^{2+} ions from aqueous solution. However, most of the previously reported chemosensors for this purpose have a number of downsides *viz.* poor detection limit, tedious synthetic procedures, intervention from other transition metal ions, long response times, use of organic solvents, and most of the reported sensors are selective only for either Ag^+ or Hg^{2+} ions (Table S1†).

Furthermore, the fluorescence sensing of cations, such as Hg^{2+}, Fe^{3+}, Pb^{2+} and Cu^{2+}, is a particularly challenging task since these ions mostly act as quenchers *via* electron transfers and facilitated intersystem crossing processes. Therefore, it remains a challenge to develop a "turn-on" fluorescence sensor for Hg^{2+} that can be applied in aqueous medium and applied to living systems. Although there are several sensors capable of recognizing Ag^+ and Hg^{2+} ions individually, to the best of our knowledge, only around 5–10% of them are selective and sensitive for both. Additionally, among the reported sensors, most of them are chemodosimeters for Hg^{2+} ions. Thus, the development of sensitive and selective methods for the determination of trace amounts of Ag^+ and Hg^{2+} ions in aqueous media is of considerable importance for both environmental protection and human health. From the literature, we also note that the presence of sulfur (as a soft Lewis base) is highly desirable in the ligands to be utilized for Ag^+ and Hg^{2+} ion recognition.

Considering the above facts and as a part of our on-going research on the design and synthesis of chemosensors,[23–27] we report herein a new pyridine substituted thiourea based sensor **PTB-1** (Scheme 1) for the selective and sensitive detection of Ag^+ and Hg^{2+} ions from 100% aqueous solution.

Results and discussion

Synthesis of PTB-1

The synthesis of **PTB-1** was achieved by using a simple nucleophilic attack by the primary amine group of pyridine to the isothiocyanato group of phenyl isothiocyanate under reflux conditions in acetone (Scheme 1).[30] The structure of **PTB-1** was characterized by IR, ^{1}H-NMR, ^{13}C-NMR spectroscopy, and HRMS spectrometry (Fig. S1–S4†). Finally, a suitable crystal of
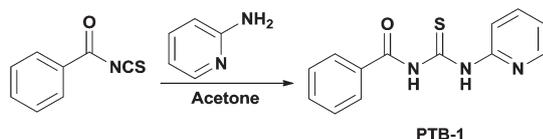
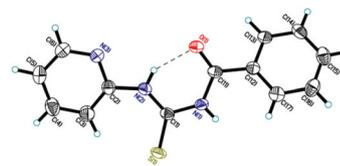**Scheme 1** Synthesis of chemosensor PTB-1.

Fig. 1 Molecular structure of **PTB-1**. Displacement ellipsoids are drawn at the 50% probability level. Selected bond lengths (Å) and angles (°): S(1)–C(1) 1.6686(18); O(1)–C(11) 1.224(2); N(1)–C(11) 1.385(2); N(1)–C(1) 1.390(2); N(1)–H(1) 0.83(2); N(2)–C(1) 1.329(2); N(2)–C(2) 1.407(2); N(2)–H(2) 0.82(2); N(3)–C(6) 1.330(3); N(3)–C(2) 1.334(3); C(11)–N(1)–C(1) 128.03(17); C(11)–N(1)–H(1) 115.4(13); C(1)–N(1)–H(1) 115.5(13); C(1)–N(2)–C(2) 133.00(17); C(1)–N(2)–H(2) 113.6(16); C(2)–N(2)–H(2) 113.3(16); O(1)–C(11)–N(1) 121.54(18); O(1)–C(11)–C(12) 121.22(16); N(1)–C(11)–C(12) 117.25(16). The intramolecular hydrogen bond is shown as a dashed line: N(2)⋯O(1) 2.592(2); N(2)–H(2)⋯O(1) 144(2).

PTB-1 for single crystal X-ray diffraction‡ was obtained from acetone, and the molecular structure is shown in Fig. 1.

Naked-eye selectivity study of PTB-1

The recognition properties of **PTB-1** were studied experimentally toward different metal ions by the naked eye, UV-visible, and fluorescence methods. During the naked-eye experiments (Fig. 2), the colorless solution of **PTB-1** [2 mL, 5×10^{-4} M, in $CH_3OH : H_2O$ (20 : 80, v/v)] turned dark brown selectively only in the presence of Ag^+ among the other tested metal ions (Cs^+, Ba^{2+}, Hg^{2+}, K^+, Li^+, Cu^{2+}, Cd^{2+}, Al^{3+}, Co^{2+}, Cr^{3+}, Mg^{2+}, Na^+, Ni^{2+}, Fe^{2+}, Fe^{3+}, Mn^{2+}, Ca^{2+}, Pb^{2+} and Zn^{2+} (200 μL, 1×10^{-2} M, in H_2O)). No significant color change of **PTB-1** was observed in the presence of the other examined cations even when present in excess, except for Hg^{2+} which exhibited a slight yellow coloration. These results clearly indicated the selective colorimetric response of **PTB-1** towards Ag^+. Furthermore, the concentration dependent naked-eye sensing of Ag^+ ions was performed (Fig. S5†), and we observed visible color changes from colorless to brown, even at a low concentration *i.e.* up to 5×10^{-4} M of Ag^+ ions. Encouraged by these Ag^+ responses shown by **PTB-1**, the qualitative and quantitative metal ion sensing ability of **PTB-1** was determined further by the use of spectrophotometric methods.

UV-visible absorption study of PTB-1

The changes in the absorption spectra of **PTB-1** in $CH_3OH : H_2O$ (20 : 80, v/v) (2 mL, 4×10^{-5} M) in the absence and presence of 5 equivalents of different metal cations (40 μL, 1×10^{-2} M, in water) are shown in Fig. 3A. The absorption bands of **PTB-1** were significantly and selectively affected by the addition of Ag^+ ions. The receptor **PTB-1** has two distinct absorption bands at 210 nm and 265 nm. Upon addition of Ag^+ ions, the absorption bands of **PTB-1** at 210 nm and 265 nm were merged together and appeared as a broad band having an absorption maximum at 243 nm along with the advent of a broad band between 350 and 600 nm. This

‡CCDC 986043† contains the supplementary X-ray data for this paper.

Fig. 2 Photograph of the vials containing **PTB-1** [2 mL, 5×10^{-4} M, in $CH_3OH : H_2O$ (20 : 80, v/v)] in the presence of 2 equivalents of different tested metal cations (200 μL, 1×10^{-2} M, in H_2O).
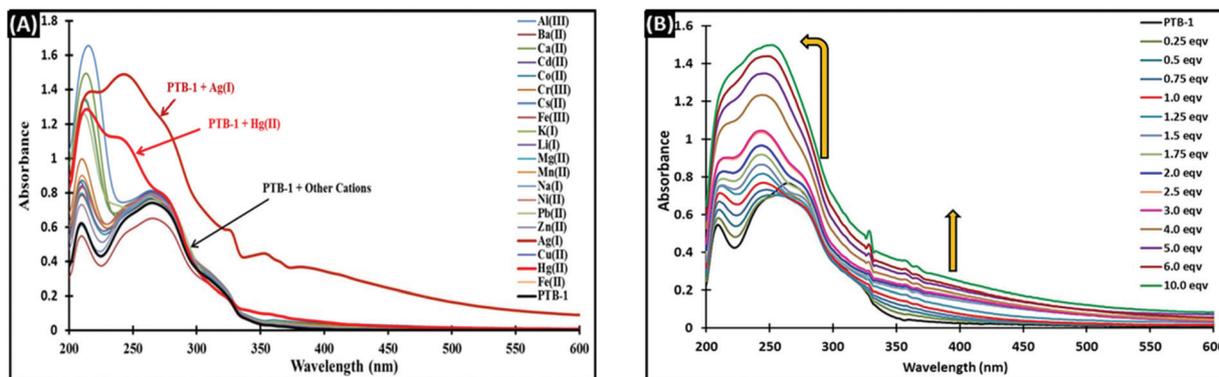

Fig. 3 UV-Vis absorption spectra of **PTB-1** (2 mL, 4×10^{-5} M) in $CH_3OH : H_2O$ (20 : 80, v/v) (A) upon addition of 5 equivalents of various metal cations (40 μL, 1×10^{-2} M, in H_2O); (B) with the successive addition of 0–10 equivalents of Ag^+ ions (1×10^{-3} M, in H_2O).

observed wide-ranging band between 350 and 600 nm is responsible for the generation of the dark brown color. A slight spectral change of **PTB-1** was observed with Hg^{2+} with the appearance of a new broad absorption band having a maximum at 214 nm. However, no noticeable spectral changes were observed with the other tested cations.

To gain more insight into the cation chemosensing properties and the mechanism of **PTB-1**, an absorption titration was performed with Ag^+ ions. As shown in Fig. 3B, upon sequential addition of Ag^+ ions (0–10 equivalent, 1×10^{-3} M, in H_2O) to the **PTB-1** solution [2 mL, 4×10^{-5} M, in $CH_3OH : H_2O$ (20 : 80, v/v)], the intensity of the absorption band centered at 243 nm was uninterruptedly amplified with the diminishing of the band at 265 nm. Also, a new broad band appeared between 350 and 600 nm. From the absorption titration data, a linear dependence of absorption at 243 nm was observed as a function of the Ag^+ concentration (Fig. S6†), and thereby the stoichiometry of **PTB-1** with Ag^+ could be estimated to be 1 : 2. Moreover, the mole ratio plot (Fig. S7†) and the Job's plot (Fig. 4) support the formation of a complex between **PTB-1** and Ag^+ in a 1 : 2 binding stoichiometry. Furthermore, direct evidence for the formation of a 1 : 2 complex was obtained from the ESI-MS spectra of **PTB-1** in the presence of 2.0 equivalents Ag^+ in methanol/water (20 : 80, v/v) (Fig. S8†). The main characteristic MS peak was observed at $m/z = 258.0714$ ([**PTB-1** + H]$^+$) for pure **PTB-1**. However, on addition of 2.0 equivalents of Ag^+, the peak at 258.0714 disappeared and a new peak appeared at $m/z = 491.2671$ corresponding to the complex [{(**PTB-1**)–2H + 2Ag} + Na]$^+$.
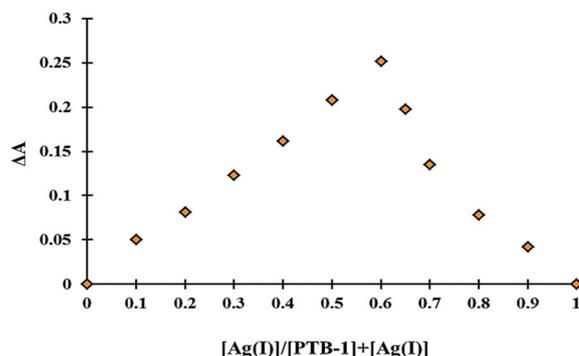
Fig. 4 Job's plot for determining the 1 : 2 stoichiometry of **PTB-1** [4×10^{-5} M, in $CH_3OH : H_2O$ (20 : 80, v/v)] and Ag^+ ions (4×10^{-5} M, in H_2O).

Based on the 1 : 2 stoichiometry for **PTB-1**·Ag^+ complexation, the binding constant (K_a) of **PTB-1** with Ag^+ was determined using the Benesi–Hildebrand plot analysis,[31] by using eqn (1).

$$\frac{1}{A - A_0} = \frac{1}{K_a(A_{max} - A_0)[Ag(I)]^2} + \frac{1}{A_{max} - A_0} \quad (1)$$

where, A and A_0 are the absorbance of the **PTB-1** solution in the presence and absence of Ag^+ ions, A_{max} is the saturated absorbance of **PTB-1** in the presence of excess amounts of Ag^+, and $[Ag^+]$ is the concentration of Ag^+ ions added (mol L^{-1}).

Finally, the plotting of $1/\Delta A$ vs. $1/[Ag^+]$ showed a linear relationship (Fig. S9†), and the binding constant (K_a) was determined from the slope and was estimated to be 15 963 M^{-1} for the **PTB-1**·Ag^+ complexation.

Furthermore, the limit of detection (LOD) and limit of quantification (LOQ) of the receptor **PTB-1** were calculated. According to the IUPAC definition, the LOD and LOQ were calculated using the relationship LOD = (3.3 × standard deviation)/slope and LOQ = (10 × standard deviation)/slope. To calculate the relative standard deviation, the absorption measurements of ten blank samples were recorded. The calibration curves (absorbance vs. $[Ag^+]$) were plotted (Fig. S6†), and then the obtained slope was used to calculate the LOD and LOQ. The obtained LOD and LOQ values of **PTB-1** for Ag^+ were found to be 3.67 μM and 0.11 μM, respectively.

Emission spectroscopic study of PTB-1

The cation binding behavior of **PTB-1** was also investigated by fluorescence spectroscopy. We observed a remarkable fluorescence enhancement of **PTB-1** [2 mL, 4 × 10^{-5} M, in CH$_3$OH : H$_2$O (20 : 80, v/v)] at 420 nm (λ_{ex} = 290 nm) upon addition of Hg^{2+} ions (40 μL, 1 × 10^{-2} M, in H$_2$O), while no significant changes were observed in the presence of other tested metal ions (Fig. 5A). The emission data of **PTB-1** with Hg^{2+} exhibited an ≈23-fold fluorescence enhancement at 420 nm. In the fluorescence titration experiment (Fig. 5B), upon the addition of increasing amounts of Hg^{2+} ions from 0 to 40 μL (0–0.5 equivalent, 1 × 10^{-3} M, in H$_2$O), the emission bands of **PTB-1** at 420 nm increased dramatically, whereas less changes in the emission intensity were observed upon the addition of 80 μL (0–1 equivalent) and a decrease was observed after the addition of 1 equivalent (80 μL) of Hg^{2+} ions to 10 equivalents (800 μL). This suggested the formation of a host–guest complex of a 2 : 1 stoichiometry. To confirm this stoichiometry, the Job's plot analysis (Fig. S10†) and the mole ratio plot (Fig. S11†) were performed. More direct evidence for the formation of this 2 : 1 complex was evaluated from the ESI-MS spectra of **PTB-1** in the presence and absence of 1.0 equivalent

of Hg^{2+} in methanol/water (20 : 80, v/v) (Fig. S12†). The peaks at m/z = 715.0420 [{2(**PTB-1**)–2H + Hg} + H]$^+$ and m/z = 258.0714 ([**PTB-1** + H]$^+$) corresponded to the complex and the receptor alone, respectively. Then, the binding constant (K_a) of **PTB-1** with Hg^{2+} was determined by a Benesi–Hildebrand plot analysis by using the fluorescence titration data (Fig. S13†). The cation binding affinity of **PTB-1** was found to be ≈100 000 M^{-1} for Hg^{2+}. Based on the fluorescence titrations, the LOD and LOQ of **PTB-1** for Hg^{2+} were found to be 0.69 nM and 0.02 nM, respectively, and these values are an improvement on reported sensors (Table S1†). Moreover, the linear response range of chemosensor **PTB-1** was calculated by plotting the ratio of fluorescence intensity vs. the increasing concentration of Hg^{2+} and Ag$^+$. The chemosensor exhibited a dynamic response range for Hg^{2+} (Fig. S14a†) from 1.0 × 10^{-7} to 1.8 × 10^{-5} M and 1.2 × 10^{-6} to 2.4 × 10^{-5} M for Ag$^+$ (Fig. S14b†).

To examine the selectivity and reversibility of **PTB-1** towards Ag$^+$ and Hg^{2+}, we carried out emission reversible titrations by using EDTA (Fig. S15†). Upon addition of an equimolar amount of EDTA solution [DMSO : H$_2$O (90 : 10, v/v)] to the solution of **PTB-1** : Hg^{2+} [4 × 10^{-5} M, in CH$_3$OH : H$_2$O (20 : 80, v/v)], the color changed from yellow to colorless and a significant decrease in the fluorescence signal at 420 nm was observed (Fig. S15a†). These results indicate that **PTB-1** detects Hg^{2+} ions reversibly. The sequential alternate addition of Hg^{2+} and EDTA solutions was repeated several times, which indicates only a slight decrease in the emission intensity, suggesting the reusability of **PTB-1** (Fig. S15b†). In contrast, the alternate addition of an equimolar amount of Ag$^+$ and EDTA solutions [DMSO : H$_2$O (90 : 10, v/v)] to the solution of **PTB-1** : Ag$^+$ [4 × 10^{-5} M, in CH$_3$OH : H$_2$O (20 : 80, v/v)] showed no change in color and fluorescence intensity (Fig. S15c and d†). These results indicate that the **PTB-1** : Ag$^+$ complexation process was irreversible with EDTA.

Possible recognition mechanism

The molecular structure of **PTB-1** and its complexes with Ag$^+$ and Hg^{2+} was computed by applying the DFT method
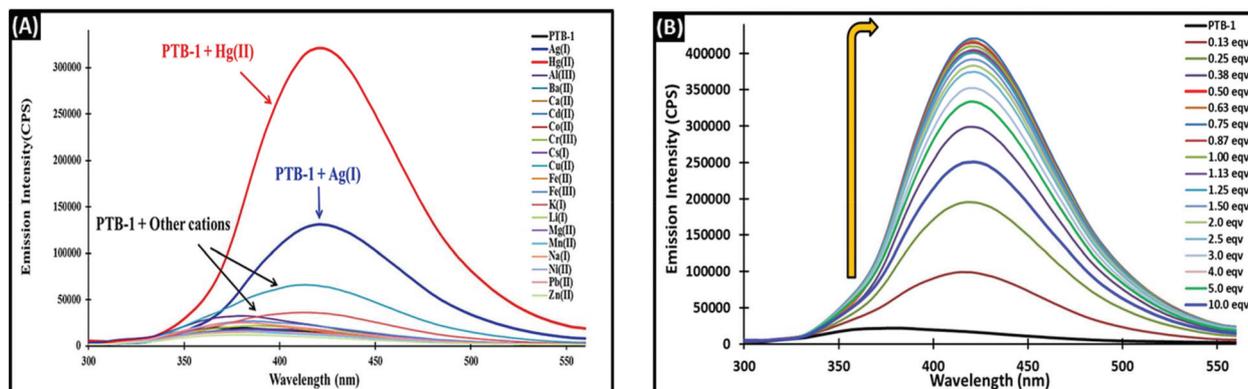

Fig. 5 Changes in the fluorescence emission intensity of **PTB-1** [2 mL, 4 × 10^{-5} M, in CH$_3$OH : H$_2$O (20 : 80, v/v)] upon the addition of (A) 5 equivalents of various cations (40 μL, 1 × 10^{-2} M, in H$_2$O), at λ_{ex} = 290 nm; (B) incremental amounts of Hg^{2+} (0–160 μL, 1 × 10^{-3} M, in H$_2$O), at λ_{ex} = 290 nm.

(Fig. S16†). The different possible binding modes of **PTB-1** with Ag$^+$ and Hg^{2+} were tested by considering the binding stoichiometry obtained from the Job's plots and other analyses. As shown in Fig. S16,† the N, S and O atoms of **PTB-1** are used on complexation with Ag$^+$, whereas a tetrahedral environment was provided by the pyridine-N and S atoms of two **PTB-1** molecules to complex with Hg^{2+}. On complexation of **PTB-1** with Ag$^+$ and Hg^{2+}, the interaction energy ($E_{int} = E_{complex} - E_{receptor} - E_{Hg^{2+}/Ag^+}$) was lowered by −390.86 kcal mol^{-1} and −263.86 kcal mol^{-1}, respectively, which indicates the formation of a stable complex. The plots of the frontier molecular orbitals of the receptor **PTB-1** and its complexes with Hg^{2+} and Ag$^+$ were analyzed (Fig. 6). The chelation of **PTB-1** with metal ions resulted in the lowering of the band gap between the highest occupied molecular orbital (HOMO) and the lowest unoccupied molecular orbital (LUMO) due to the intramolecular charge transfer (ICT), which may be responsible for the naked-eye detectable color change and the appearance of a new absorption spectral band in the visible region. Also, the calculated band gap of the **PTB-1**·(Ag$^+$)$_2$ complex was found to be lower than the (**PTB-1**)$_2$·Hg^{2+} complex. These calculated results correlated well with the metal ion selectivity observed by UV-Vis absorption spectroscopy. Furthermore, to understand the fluorescence enhancement of **PTB-1** with Hg^{2+}, the electron density distribution of the HOMO and LUMO in **PTB-1** and the (**PTB-1**)$_2$·Hg^{2+} complex was analyzed. In the free receptor, the HOMO was localized mainly over the S atom and the LUMO was distributed uniformly over the receptor which allowed for the photoinduced electron transfer (PET) process from the chelating moiety to the fluorophore moiety. Upon complexation with Hg^{2+}, the electron density over the S atom of **PTB-1** was transferred to the Hg^{2+} ions which inhibited the possibility of fluorescence quenching through PET in the (**PTB-1**)$_2$·Hg^{2+} complex.

Furthermore, we carried out ^{1}H NMR spectroscopic titration experiments on **PTB-1** solutions with various equivalents of Hg^{2+} and Ag$^+$ ions separately (Fig. S17 and S18†). Upon addition of 0.5 equiv. of Hg^{2+} ions, it was observed that the peaks due to the two NH protons of **PTB-1** at 13.12 and 9.07 ppm disappeared, whilst a broad peak appeared at

16.13 ppm probably due to the OH group (Fig. S17†). In addition, some of the aromatic protons of **PTB-1** exhibited an up-field shift (from 8.83, 8.46 and 7.78 ppm to 8.46, 8.05 and 7.67 ppm, respectively) while some other aromatic protons exhibited a down-field shift (from 7.92, 7.54 and 7.18 to 8.06, 7.58 and 7.32 ppm, respectively) in the presence of Hg^{2+} ions accompanied by a broadening of the peaks. Similar NMR studies conducted on **PTB-1** by adding various equivalents of Ag$^+$ also exhibited the disappearance of both the NH protons of **PTB-1** at 13.12 and 9.07 ppm (Fig. S18†); 2.0 equiv. of Ag$^+$ ions are required for the complete disappearance of these peaks. However, in contrast to the case of Hg^{2+} addition, no broad peak at 16.12 ppm appeared upon addition of Ag$^+$ ions. In addition, some of the aromatic protons of **PTB-1** revealed an up-field shift (from 8.83 and 8.46 ppm to 8.37 and 8.06 ppm, respectively) whilst others exhibited a down-field shift (from 7.92, 7.54 and 7.18 ppm to 7.99, 7.59 and 7.51 ppm, respectively) upon addition of Ag$^+$ ions, which was accompanied by broadening of peaks. It is noteworthy that some aromatic protons of **PTB-1** experience a slight net increase in shielding which may be attributed to the anisotropic effect and conformation changes after coordination with Hg^{2+} or Ag$^+$.[33]

Direct evidence for the formation of complexes of **PTB-1** with Hg^{2+} and Ag$^+$ was obtained from HR-MS analysis. The HR-MS spectra of pure **PTB-1** exhibited a characteristic MS peak at $m/z = 258.0714$ corresponding to [(**PTB-1**) + H]$^+$ (Fig. S4†). However, upon addition of 0.5 equivalents of the Hg^{2+} ion, a new peak appeared at $m/z = 715.0420$, corresponding to the species [{2(**PTB-1**) − 2H + Hg} + H]$^+$, which confirmed the formation of a 2:1 complex of **PTB-1** with the Hg^{2+} ion (Fig. S12†). Similarly, upon addition of 2.0 equivalents of Ag$^+$, the parent ion peak of **PTB-1** at $m/z = 258.0714$ disappeared and a new peak appeared at $m/z = 491.2671$ corresponding to the species [{(**PTB-1**) − 2H + 2Ag} + Na]$^+$, suggesting the formation of a 1:2 complex (Fig. S8†). Additionally, FT-IR comparative studies of **PTB-1** and the **PTB-1**·Hg^{2+} complex were performed (Fig. S19†). The shifting of the –NH, C=S and C=O bands also supports the proposed binding mechanism.
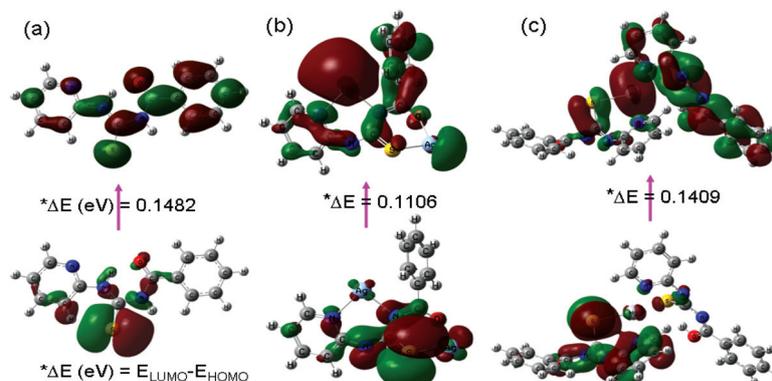

Fig. 6 The DFT computed LUMO (above) and HOMO (below) diagrams of (a) **PTB-1** and its (b) **PTB-1**·(Ag$^+$)$_2$ and (c) (**PTB-1**)$_2$·Hg^{2+} complexes.

Interference and pH effects

The UV-Vis and emission responses of receptor **PTB-1** to various possible interfering metal ions and its selectivity for Ag^+ and Hg^{2+} ions were tested. To study this, two equivalents of Ag^+ and Hg^{2+} ions (16 μL, 1×10^{-2} M, in H_2O) were added to the solution containing **PTB-1** [4×10^{-5} M, in $CH_3OH : H_2O$ (20 : 80, v/v)] and two equivalents of the other competitive metal ions (16 μL, 1×10^{-2} M, in H_2O) of interest; their absorption and emission spectra were recorded. From the absorption study, the Ag^+ selectivity of **PTB-1** was not affected by the presence of the other tested ions, including Hg^{2+} (Fig. 7A). Similarly, the fluorescent sensing of Hg^{2+} by chemosensor **PTB-1** was found to be barely affected by a number of commonly co-existing miscellaneous competitive cations, including Ag^+ (Fig. 7B). Additionally, the UV-Vis and fluorescence responses of the sensor **PTB-1** in acidic and basic pH regions were examined. It was observed that the optimum pH range for the use of **PTB-1** for detecting Ag^+ and Hg^{2+} ions was 5–9.

Test strips and supported silica based applications of PTB-1

In order to ensure that **PTB-1** is potentially of practical use, **PTB-1** loaded test strips were prepared to detect Ag^+ ions from an aqueous environment. The desired test strips were prepared by soaking small strips of cellulose paper (Whatman No. 42) in the solution of **PTB-1** (1×10^{-2} M) in methanol and were dried in air. When these strips were treated with 10 mL aqueous solution of Ag^+ (1×10^{-4} M), the colorless strips sharply turned dark brown (Fig. 8A and ESI video†). The rapid color change of the test strip in solution clearly inferred the practical application of **PTB-1**. To evaluate the applicability of the **PTB-1** loaded test strips for the quantitative determination of Ag^+ in aqueous solution, the test strips were immersed at different concentrations of Ag^+ showing a clear color change (Fig. S20†). The detection limit of the test strips was found to be 1×10^{-6} M, allowing for the sensitive detection of Ag^+ ions.

The sensing of Ag^+ by **PTB-1** also worked on a solid support. The silica gel (60–120 mesh, 5.0 g, colorless) was
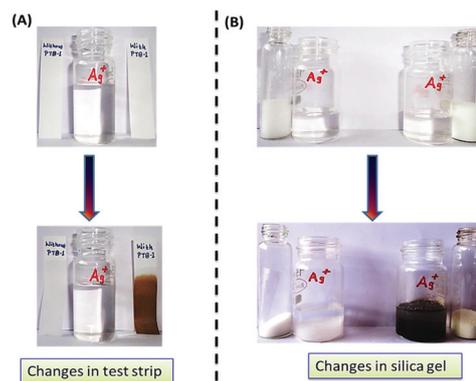

Fig. 8 Practical application of **PTB-1** for the detection of Ag^+ by (A) the test strip method and (B) the silica support method.

soaked in **PTB-1** (in methanol, 5 mL, 1×10^{-2} M) and then the solvent was removed. A very faint off-white color for the silica gel appeared, which indicated the adsorption of the receptor on the surface. When it was treated with 10 mL aqueous solution of Ag^+ (1×10^{-4} M), the colorless solution promptly turned dark brown (Fig. 8B & ESI video†). The instantaneous color change of the solid silica gel in solution clearly inferred the practical application of **PTB-1** for the qualitative detection of Ag^+ in aqueous media.

Live cell imaging study of PTB-1

The fluorescent behavior of **PTB-1** was applied to the intracellular detection and monitoring of Hg^{2+} in a HepG2 liver cell line *i.e.* the human hepatocellular liver carcinoma cell line. After being incubated with **PTB-1** (10 μM) in RPMI 1640 for 20 min, the cells were imaged by using a confocal fluorescence microscope as shown in Fig. 9A. As expected, no fluorescent image was observed. Then, the HepG2 cells loaded with **PTB-1** were incubated with 100 μM of Hg^{2+} for 0.5 h in RPMI 1640 medium at 37 °C, and then washed with RPMI 1640 to remove excess Hg^{2+} ions and were imaged (Fig. 9C). As shown
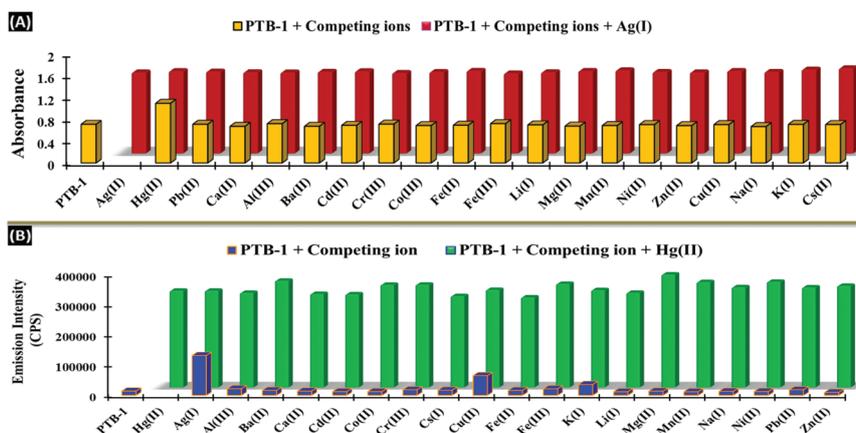

Fig. 7 Competitive (A) absorbance response of **PTB-1** and **PTB-1**:Ag^+ complex at 243 nm, (B) fluorescence response of **PTB-1** and **PTB-1**:Hg^{2+} complex at 420 nm in presence of different metal cations.
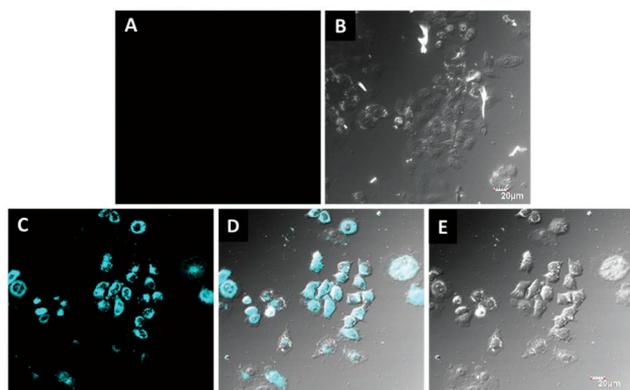
Fig. 9 Fluorescence confocal microscopy images of living HepG2 cells incubated with Hg^{2+}: (A) cells loaded with 10 μM of **PTB-1** for 20 min as a control, (C) cells in 'A' loaded with Hg^{2+} 100 μM for 0.5 h, (D) overlay of fluorescence channels in 'C', (B and E) bright field images of 'A' and 'C', respectively. The scale bar is 20 μm.

in Fig. 9C and D, there was a significant increase in the intracellular fluorescence emission intensity compared to the control cells as shown in Fig. 9A and B, which indicated the ability of **PTB-1** to detect intracellular Hg^{2+} ions. Moreover, the fluorescence stability of **PTB-1** and **PTB-1** + 0.5 equiv. of Hg(II) [(2 mL, 4×10^{-5} M) in $CH_3OH : H_2O$ (20 : 80, v/v)] was also evaluated (Fig. S21†), and the fluorescence intensity hardly changed over 3 h. On this basis, we suggested that **PTB-1** had good fluorescence stability.

To access the potential toxicity of **PTB-1**,[34] MTT assays were carried out. HepG2 cells (10^6 cells per mL) were planted into 96-well microtiter plates in DMEM with 10% fetal bovine serum (FBS). Plates were maintained at 37 °C in a 5% CO_2/95% air incubator for 12 h. Then the cells were incubated for 24 h at 37 °C in the 5% CO_2/95% air incubator with different concentration probes of 0 μM to 100 μM, respectively. MTT solution (5.0 mg mL^{-1}, PBS) was then added to each well. After 4 h, the remaining MTT solution was removed, and 200 μL of DMSO was added to each well, followed by shaking for 10 min to dissolve the formazan crystals at room temperature. Absorbance was measured at 490 nm using a TECAN infinite M200pro microplate reader. The high cell viability of **PTB-1** indicated that the probe displayed low cytotoxicity to living cells (Fig. S22†).

Crystal structure of PTB-1

The pyridine substituted thiourea fragment (C_5H_4N)–NH–C(=S)–NH–C(=O)– is planar within 0.103(1) Å (Fig. 1). This conformation is stabilized by a short intramolecular hydrogen bond N(2)–H(2)···O(1) with an N···O separation of 2.592(2) Å. The phenyl ring C(12)–C(17) is slightly skewed around the C(11)–C(12) bond; the torsion angle O(1)–C(11)–C(12)–C(13) is equal to 25.6(3)°. According to the Cambridge Structural Database,[32] all the bond lengths and angles in this structure exhibit ordinary values. In the structure, adjacent molecules are connected as centrosymmetric dimers via N(1)–H(1)···S(1) hydrogen bonds (Fig. S23†).

Experimental

Materials and measurements

All the starting reagents and metal perchlorates were purchased either from S.D. Fine chemicals or Sigma Aldrich depending on their availability, and were used as received. All the solvents were of spectroscopic grade and were used without further treatment. The purity of the compounds and the progress of reactions were determined and monitored by means of analytical thin layer chromatography (TLC). Precoated silica gel 60 F_{254} (Merck) on alumina plates (7 × 3 cm) were used and visualized by using either an iodine chamber or a short UV-visible lamp. Melting points were recorded on the Celsius scale by the open capillary method and are uncorrected. IR spectra were recorded on a PerkinElmer Spectrum One FT-IR spectrometer as potassium bromide pellets and Nujol mulls, unless otherwise mentioned. IR bands are expressed in frequency (cm^{-1}). The ^1H and ^{13}C NMR spectra were recorded on a Jeol JNM-ECX 500 MHz multinuclear probe NMR spectrometer at ambient temperature in DMSO with TMS as an internal standard and chemical shifts are reported in ppm. The abbreviations s, d and t stand for singlet, doublet and triplets, respectively. Mass spectra were recorded on a Bruker Compact HD mass spectrometer. UV-Vis spectra were recorded on a U-3900 spectrophotometer (PerkinElmer Co., USA) with a quartz cuvette (path length = 1 cm). Fluorescence spectra were recorded on a Fluoromax-4 spectrofluorometer (HORIBA JobinYvon Co., France).

Synthesis of PTB-1. In a 100 mL three necked flask fitted with a reflux condenser and a dropping funnel, ammonium thiocyanate (5.0 g, 0.0656 mol) in 25 mL of dry acetone was placed. To this solution, benzoyl chloride (9.23 g, 0.0656 mol) in 10 mL of dry acetone was added dropwise using a dropping funnel. After completion of the addition, the reaction mixture was refluxed for 15 to 20 min. To this refluxed solution, 2-amino pyridine (6.18 g, 0.0656 mol) dissolved in 15 mL of dry acetone was added dropwise. Refluxing was continued for 2 h, and the reaction progress was monitored by TLC. After completion of the reaction, the reaction mixture was cooled to room temperature and was poured into ice cold water with vigorous stirring. The yellow colored solid was filtered, washed with cold water (3 × 20 mL) to give a crude product. The pure **PTB-1** was afforded after recrystallization from acetone. Yield: 91%; mol. formula: $C_{13}H_{11}N_3OS$; mol. weight: 257.06 g; physical nature: yellow solid; m.p.: 108–110 °C; IR (cm^{-1}) [KBr]: 3277, 3224, 3005, 1678, 1597, 1550, 1438, 1284, 1251, 1157, 1109, 885; ^1H NMR (500 MHz, $CDCl_3$, δ ppm): 7.18 (t, J = 7.5 Hz, 1H, Ar–H), 7.54 (t, J = 7.5 Hz, 2H, Ar–H), 7.65 (t, J = 7.5 Hz, 1H, Ar–H), 7.78 (t, J = 7.5 Hz, 1H, Ar–H), 7.92 (d, J = 10.0 Hz, 2H, Ar–H), 8.46 (d, J = 5.0 Hz, 1H, Ar–H), 8.83 (d, J = 10 Hz, 1H Ar–H), 9.07 (s, 1H, NH), 13.12 (s, 1H, NH); ^{13}C NMR (125 MHz, $CDCl_3$, δ ppm): 116.0, 121.4, 127.5, 129.2, 131.6, 133.7, 137.69, 148.6, 151.2, 166.4, and 176.9; HRMS (ESI): m/z: calculated for $C_{13}H_{11}N_3OS$: $[M + H]^+$ 258.06, found: 258.0714.

X-ray diffraction studies. Crystal data of **PTB-1**: $C_{13}H_{11}N_3O_1S_1$, M = 257.31, monoclinic, a = 5.2573(8), b =

20.338(3), $c = 11.7359(17)$ Å, $\beta = 90.393(2)°$, $V = 1254.8(3)$ Å^3, space group $P2_1/n$, $Z = 4$, $D_c = 1.362$ g cm^{-3}, $F(000) = 536$, $\mu(MoK_\alpha) = 0.249$ mm^{-1}, colorless plate with dimensions *ca.* $0.32 \times 0.09 \times 0.01$. A total of 8081 reflections (2343 unique, $R_{int} = 0.0418$) were measured on a Bruker SMART APEX II diffractometer (graphite monochromatized MoK$_\alpha$ radiation, $\lambda = 0.71073$ Å) using ω-scan mode at 150 K. The structure was solved by direct methods and refined by full matrix least-squares on F^2 with anisotropic thermal parameters for all non-hydrogen atoms.[28] All H atoms were found from difference Fourier synthesis and refined isotropically. The final residuals were $R_1 = 0.0373$, w$R_2 = 0.0797$ for 1720 reflections with $I > 2\sigma(I)$ and 0.0628, 0.0886 for all data and 207 parameters. GooF = 1.006, maximum $\Delta\rho = 0.229$ e Å^{-3}.

Computational methods. The Gaussian 09W computer program was used for all theoretical calculations.[29] The optimization of **PTB-1** and its complexes with Ag$^+$ and Hg^{2+} was carried out without symmetry constraints by applying the B3LYP/6-31G(d,p) method in the gas phase. The basis set LANL2DZ was used for Ag and Hg atoms.

Spectroscopic study. The aqueous stock solutions of cations of concentration 1×10^{-2} mol L^{-1} were prepared from their corresponding salts *i.e.* AgClO$_4$, Al(ClO$_4$)$_3$·9H$_2$O, Ba(ClO$_4$)$_2$, Ca(NO$_3$)$_2$·4H$_2$O, Cd(ClO$_4$)$_2$·H$_2$O, Co(ClO$_4$)$_2$·6H$_2$O, Cr(ClO$_4$)$_3$·6H$_2$O, CsNO$_3$, KNO$_3$, NaNO$_3$, Fe(ClO$_4$)$_2$·xH$_2$O, HgCl$_2$, LiBr, Mg(ClO$_4$)$_2$, Mn(ClO$_4$)$_2$·H$_2$O, Ni(ClO$_4$)$_2$·6H$_2$O, Fe(ClO$_4$)$_3$·H$_2$O, Pb(ClO$_4$)$_2$·3H$_2$O, Zn(ClO$_4$)$_2$·6H$_2$O and Cu(ClO$_4$)$_2$·6H$_2$O. These solutions were used for all spectroscopic studies after appropriate dilution. The stock solution of **PTB-1** (1.0×10^{-2} mol L^{-1}) was prepared in methanol and then diluted to 4×10^{-5} mol L^{-1} with CH$_3$OH : H$_2$O (20 : 80, v/v) mixed solvents. For the spectroscopic (UV-Vis and fluorescence) titrations, the required amount of the diluted receptor **PTB-1** [2 mL, 4×10^{-5} mol L^{-1}, in CH$_3$OH : H$_2$O (20 : 80, v/v)] was taken directly into a cuvette and the spectra were recorded after each successive addition of cations (0–240 μL, 1×10^{-3} mol L^{-1}, in H$_2$O) by using a micropipette. The interaction of **PTB-1** with Ag$^+$ and Hg^{2+} ions was completed in less than 2 minutes, and therefore all readings were taken 2 minutes after the addition.

Living cell imaging. The solution of **PTB-1** (DMSO, 1.0 mM) was maintained in a refrigerator at 4 °C. HgCl$_2$ was used as the Hg^{2+}-supplemented source. The HepG2 cells (human hepatocellular liver carcinoma cell line) were purchased from the Committee on type Culture Collection of Chinese Academy of Sciences. Cells were seeded at a density of 1×10^6 cells per mL for confocal imaging in RPMI 1640 medium supplemented with 20% fetal bovine serum (FBS), NaHCO$_3$ (2 g L^{-1}), and 1% antibiotics (penicillin/streptomycin, 100 U ml^{-1}). Cultures were maintained at 37 °C under a humidified atmosphere containing 5% CO$_2$. The cells were sub-cultured by scraping and seeding on 15 mm Petri-dishes according to the instructions from the manufacturer. The fluorescent images of cells were acquired on an 'Olympus laser-scanning microscope' with an objective lens (×40). The excitation of **PTB-1** was carried out using a laser at 351 nm and emission was collected between 400 and 500 nm. Prior to imaging, the medium was removed.

Cell imaging was carried out after washing the cells with RPMI-1640 three times.

Conclusions

In conclusion, we have synthesized and developed a simple thiourea based colorimetric Ag$^+$ selective and fluorescent 'turn-on' Hg^{2+} selective sensor **PTB-1**. Sensor **PTB-1** exhibited an excellent selectivity for Ag$^+$ and Hg^{2+} ions over other possible interfering metal ions with a detection limit down to micromolar (3.67 μM) and nanomolar (0.69 nM) concentrations, respectively. The sensor **PTB-1** recognized Ag$^+$ and Hg^{2+} with a 1 : 2 and 2 : 1 binding stoichiometry, respectively. Confocal microscopy images indicate that **PTB-1** can be used for detecting changes in Hg^{2+} levels within living cells. Also, **PTB-1** can be applied for the colorimetric detection of Ag$^+$ in the aqueous media by the naked eye using test strip and silica support methods.

Conflicts of interest

There are no conflicts of interest.

Acknowledgements

References

1 M. Formica, V. Fusi, L. Giorgi and M. Micheloni, *Coord. Chem. Rev.*, 2012, **256**, 170–192.

2 M. E. Jun, B. Roy and K. H. Ahn, *J. Chem. Soc., Chem. Commun.*, 2011, **47**, 7583–7601.

3 H. N. Kim, W. X. Ren, J. S. Kim and J. Yoon, *Chem. Soc. Rev.*, 2012, **41**, 3210–3244.

4 E. M. Nolan and S. J. Lippard, *Chem. Rev.*, 2008, **108**, 3443–3480.

5 (*a*) E. B. Veale and T. Gunnlaugsson, *Annu. Rep. Prog. Chem., Sect. B: Org. Chem.*, 2010, **106**, 376–406; (*b*) Y. Ding, W. Zhu and Y. Xie, *Chem. Rev.*, 2017, **4**, 2203–2256; (*c*) Y. Ding, Y. Tang, W. Zhu and Y. Xie, *Chem. Soc. Rev.*, 2015, **44**, 1101–1112; (*d*) B. Chen, Y. Ding, X. Li, W. Zhu, J. P. Hill, K. Ariga and Y. Xie, *Chem. Commun.*, 2013, **49**, 10136–10138; (*e*) Y. Ding, X. Li, T. Li, W. Zhu and Y. Xie, *J. Org. Chem.*, 2013, **78**, 5328–5338.

6 H. T. Ratte, *Environ. Toxicol. Chem.*, 1999, **18**, 89–108.

7 Q. L. Feng, J. Wu, G. Q. Chen, F. J. Cui, T. N. Kim and J. O. Kim, *J. Biomed. Mater. Res.*, 2000, **52**, 662–668.

8 A. B. G. Lansdown, *J. Wound Care*, 2002, **11**, 125–130.

9 M. Yamanaka, K. Hara and J. Kudo, *Appl. Environ. Microbiol.*, 2005, **71**, 7589–7593.

10 M. K. Aminia, M. Ghaedia, A. Rafia, I. Mohamadpoor-Baltorka and K. Niknam, *Sens. Actuators, B*, 2003, **96**, 669–676.

11 A. S. Craig, R. Kataky, R. C. Mattews, D. Parker, G. Feruson, A. Lugh, H. Adams, N. Bailey and H. Schneider, *J. Chem. Soc., Perkin Trans. 2*, 1990, 1523–1531.

12 A. S. Craig, R. Kataky, D. Parker, H. Adams, N. Bailey and H. Schneider, *J. Chem. Soc., Chem. Commun.*, 1989, 1870–1872.

13 EPA Mercury Update Impact on Fish Advisories, EPA Fact Sheet EPA-823-F-01-011; EPA, Office of Water, Washington, DC, **2001**. pp. 1–10.

14 S. D. Richardson and T. A. Temes, *Anal. Chem.*, 2005, **77**, 3807–3838.

15 G. H. Scoullos, M. J. Vonkeman, L. Thorton and Z. Makuch, in *Mercury, Cadmium, and Lead: Handbook for Sustainable Heavy Metals Policy and Regulation (Environment & Policy)*, Kluwer Academic, Norwell, MA, 2001, vol. 31.

16 C. C. Huang and H. T. Chang, *Anal. Chem.*, 2006, **78**, 8332–8338.

17 P. B. Tchounwou, W. K. Ayensu, N. Ninashvili and D. Sutton, *Environ. Toxicol.*, 2003, **18**, 149–175.

18 F. Wang, S. W. Nam, Z. Guo, S. Park and J. Yoon, *Sens. Actuators, B*, 2012, **161**, 948–953.

19 W. Zheng, M. Aschner and J. F. Ghersi-Egea, *Toxicol. Appl. Pharmacol.*, 2003, **192**, 1–11.

20 D. Kagan, P. C. Marzal, S. Balasubramanian, S. Sattayasamitsathit, K. M. Manesh, G. U. Flechsig and J. Wang, *J. Am. Chem. Soc.*, 2009, **131**, 12082–12083.

21 D. Karunasagar, J. Arunachalam and S. J. Gangadharan, *J. Anal. At. Spectrom.*, 1998, **13**, 679–682.

22 Y. Li, C. Chen, B. Li, J. Sun, J. Wang, Y. Gao, Y. Zhao and Z. Chai, *J. Anal. At. Spectrom.*, 2006, **21**, 94–96.

23 J. P. Nandre, S. Patil, V. Patil, F. Yu, L. Chen, S. Sahoo, T. Prior, C. Redshaw, P. Mahulikar and U. Patil, *Biosens. Bioelectron.*, 2014, **61**, 612–617.

24 S. R. Patil, J. P. Nandre, D. Jadhav, S. Bothra, S. K. Sahoo, M. Devi, C. P. Pradeep, P. P. Mahulikar and U. D. Patil, *J. Chem. Soc., Dalton Trans.*, 2014, 13299–13306.

25 M. Chandel, S. M. Roy, D. Sharma, S. K. Sahoo, A. Patel, P. Kumari, R. S. Dhale, K. S. K. Ashok, J. P. Nandre and U. D. Patil, *Luminescence*, 2014, **154**, 515–519.

26 A. K. Gupta, A. Dhir and C. P. Pradeep, *J. Chem. Soc., Dalton Trans.*, 2013, **42**, 12819–12823.

27 D. Sharma, A. Moirangthem, S. K. Sahoo, A. Basu, S. M. Roy, R. K. Pati, K. S. K. Ashok, J. P. Nandre and U. D. Patil, *RSC Adv.*, 2014, **4**, 41446–41452.

28 G. M. Sheldrick, *Acta Crystallogr., Sect. A: Fundam. Crystallogr.*, 2008, **64**, 112–122.

29 H. B. Schlegel, G. E. Scuseria, M. A. Robb, J. R. Cheeseman, G. Scalmani, V. Barone, B. Mennucci, G. A. Petersson, H. Nakatsuji, M. Caricato, X. Li, H. P. Hratchian, A. F. Izmaylov, J. Bloino, G. Zheng, J. L. Sonnenberg, M. Hada, M. Ehara, K. Toyota, R. Fukuda, J. Hasegawa, M. Ishida, T. Nakajima, Y. Honda, O. Kitao, H. Nakai, T. Vreven, J. A. Montgomery Jr. J. E. Peralta, F. Ogliaro, M. Bearpark, J. J. Heyd, E. Brothers, K. N. Kudin, V. N. Staroverov, R. Kobayashi, J. Normand, K. Raghavachari, A. Rendell, J. C. Burant, S. S. Iyengar, J. Tomasi, M. Cossi, N. Rega, J. M. Millam, M. Klene, J. E. Knox, J. B. Cross, V. Bakken, C. Adamo, J. Jaramillo, R. Gomperts, R. E. Stratmann, O. Yazyev, A. J. Austin, R. Cammi, C. Pomelli, J. W. Ochterski, R. L. Martin, K. Morokuma, V. G. Zakrzewski, G. A. Voth, P. Salvador, J. J. Dannenberg, S. Dapprich, A. D. Daniels, O. Farkas, J. B. Foresman, J. V. Ortiz, J. Cioslowskiand and D. J. Fox, *Gaussian 09, Revision A.1*, Gaussian, Inc., Wallingford CT, 2009.

30 R. L. Frank and P. V. Smith, *Org. Synth.*, 1948, **28**, 89–90.

31 H. A. Benesi and J. H. Hildebrand, *J. Am. Chem. Soc.*, 1949, **71**, 2703–2707.

32 F. H. Allen, *Acta Crystallogr., Sect. B: Struct. Sci.*, 2002, **58**, 380–388.

33 (*a*) M. Alfonso, A. Espinosa, A. Tarraga and P. Molina, *ChemistryOpen*, 2014, **3**, 242–249; (*b*) A. Misra, M. Shahid, P. Srivastava and P. Dwivedi, *J. Inclusion Phenom. Macrocyclic Chem.*, 2011, **69**, 119–129.

34 F. Adhami, M. Safavi, M. Ehsani, S. K. Ardestani, F. Emmerling and F. Simyari, *Dalton Trans.*, 2014, **43**, 7945–7957.